SPECIAL ISSUE ARTICLE

WILEY

Diversion of the paleo-Yellow River channel in the Qingtongxia area of Ningxia, China: Evidence from terraces and fluvial landforms

Hong Chen[1,2] | Guo-dong Bao[1] | Wei Shi[1,2] | Jian-min Hu[1,2]

[1] Institute of Geomechanics, Chinese Academy of Geological Sciences, Beijing, China

[2] Key Laboratory of Paleomagnetism and Tectonic Reconstruction of Ministry of Natural Resources, Beijing, China

Correspondence
Hong Chen, Institute of Geomechanics, Chinese Academy of Geological Sciences, No.11 Minzudaxue South Road, Haidian District. Beijing 100081, China.
Email: chhzxm8281@163.com

The Qingtongxia Grand Canyon (QGC) of the Yellow River is a region of intense tectonic deformation that is located in the southern Yinchuan Basin, at the junction of the western margin of the Ordos Plateau and the northeast arcuate structural belt of the Qinghai–Tibetan Plateau. The Yellow River makes a 90° turn as it traverses the Qingtongxia area, incising the hard Ordovician sandstones of Niushou Mountain, while leaving the relatively soft Quaternary sediments on the northern side of the channel undisturbed. Despite this apparent inconsistency with the expected pattern of river erosion, there has been no significant research to date on the formation of the QGC. Here, we utilize remote sensing, surficial geomorphology, and shallow coring to confirm the evolution of the Yellow River channel and formation of the QGC. Using Landsat Thermic Mapper and ASTER imagery, we identified a N–S-oriented zone of high water-content in the northern part of the QGC that is characterized at the surface by marsh and wetlands. Shallow cores reveal the zone is underlain by Yellow River gravel, while seismic profiling confirms anomalous seismic structures relative to the surrounding strata. Together, these data document a paleo-Yellow River channel in the northern Qingtongxia area. We selected four representative profiles of the Yellow River terraces in the Qingtongxia and adjacent areas to acquire measurements on above water level and age. The uppermost terraces preserved at the entrance, central section, and exit of the QGC are labelled T6, T9, and T3, respectively. Our data indicate that the flow direction during the construction of T9 was different to that of the modern Yellow River and that canyon incision occurred during the development of T3, which we constrain to 65–85 ka. Ultimately, we (a) document a paleo-Yellow River channel north of the QGC, which may have been affected by tectonic activity since the late Pleistocene and (b) show that the Yellow River has since been diverted towards the Yinchuan Basin via the QGC.

KEYWORDS

Niushou Mountain, paleo-river channel. Qingtongxia Grand Canyon, terrace, Yellow River

1 | INTRODUCTION

The Qingtongxia Grand Canyon (QGC) of North China is the most eastern gorge in the upper reaches of the Yellow River. Flowing from south to north along the western piedmont of Niushou Mountain, the Yellow River incises a Z-shape to form the approximately 10-km-long canyon (Figures 1 and 2). Local lithologies are dominated by loose Cenozoic sandstones and mudstones to the west and north of the river (Liang
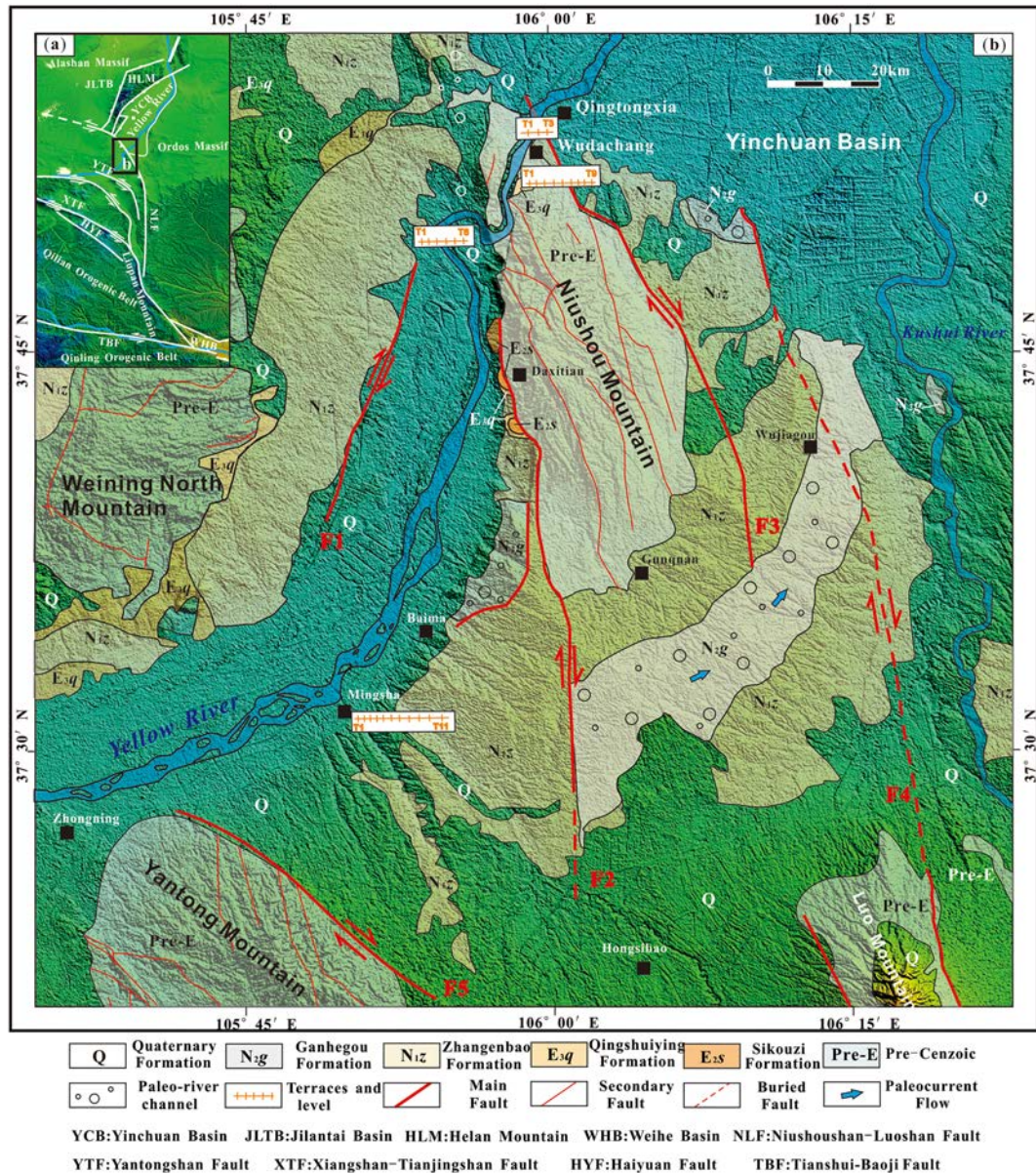
FIGURE 1 Geological map of the study region (modified form Liang et al., 2013 and Chen et al., 2015) [Colour figure can be viewed at wileyonlinelibrary.com]

et al., 2013; Zhou, Yao, & Wang, 1994) and by hard Ordovician sandstones derived from the Niushou Mountain massif to the east (Geological Survey Institute of Ningxia Hui Autonomous Regio, 2018). Paradoxically, the Yellow River did not continue its northward course through the relatively soft Cenozoic strata at the head of the gorge, but instead turned south to follow the western boundary of Niushou Mountain for 2 km and then forming a feature known as the QGC, before crossing the geologic boundary and incising into the more resistant bedrock. In this way, the formation of the QGC appears to be inconsistent with the fundamental geological and geomorphological characteristics of the surrounding area.

The natural evolution of river channels is a highly complex process, governed by a number of factors, including lithology (Hooke, 1979, 1980) and rock compaction (Lawler, 1992, 1995; Lawler, Couperthwaite, Bull, & Harris, 1997; Trimble, 1994) on both sides of the river, channel geometry (Knighton, 1998; Laubel, Kronvang, Hald, & Jensen, 2003; Lawler, 1995; Lawler et al., 1997), hydrodynamics, vegetation cover, and climate. However, the Yellow River channel developed in a fashion that appears to be counter-intuitive in the northern QGC, resulting in incision of the highly resistant Niushou Mountain sandstone, instead of the uncompacted and poorly cemented Cenozoic sediments.

River bend development is also influenced by external factors, such as bedrock barriers and tectonic activity (Potter, 1978; Peltzer, Tapponnier, Zhang, & Xu, 1985; Zhang et al., 1988; Jackson, Norris, & Youngsun, 1996; Lacassin, Replumaz, Leloup, & Herv, 1998; Lin, Maruyama, & Miyata, 1998; Maruyama & Lin, 2000; Schumm, Dumont, & Holbrook, 2000). For example, compressional tectonics along the northeastern margin of the Qinghai–Tibetan Plateau resulted in the Yellow River making a "π" curve around the Ordos
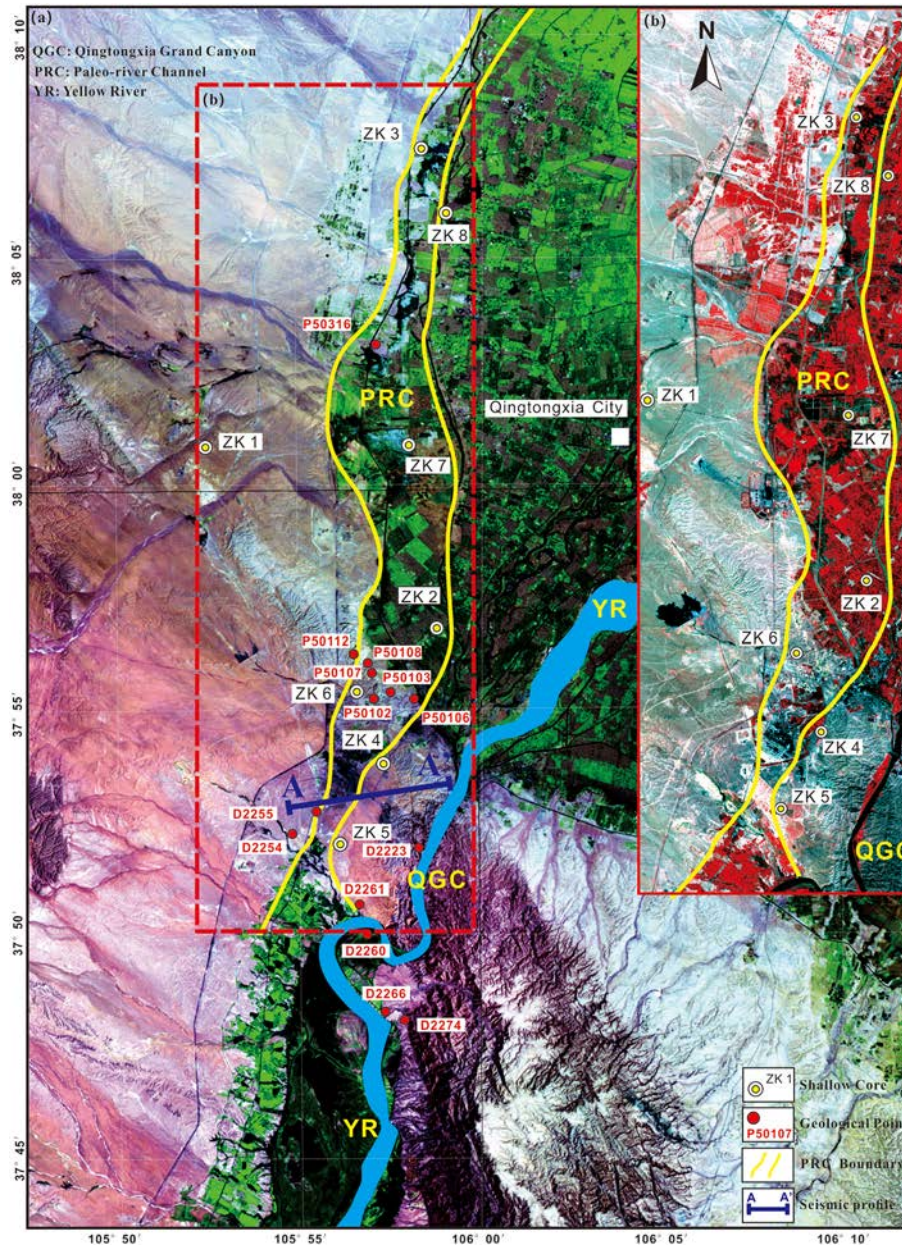
FIGURE 2 Physiognomy of the paleo-river channel in the Qingtongxia area. Data are primarily derived from Thermic Mapper (a) and ASTER (b) imagery [Colour figure can be viewed at wileyonlinelibrary.com]

Block (Chen, Fan, Zhang, & Fan, 2013; Lin, Yang, Sun, & Yang, 2001), while the multiple π bends in the Shapotou area are the products of left-lateral strike-slip dislocation of Xiangshan–Tianjingshan, coupled with the endogenous dynamics of the Yellow River (Jiang, Yin, Yu, & Wang, 2013). Similarly, the initial bend in the Yangtze River in the southeastern Qinghai–Tibetan Plateau is due to orogenic uplift (Shen et al., 2016), while the hairpin rivers characteristic of southeast Asia is linked to tectonic activity (Lacassin et al., 1998). One of the world's largest river systems, the Yellow River originates at the northeastern margin of the tectonically active Qinghai–Tibetan Plateau and is offset along its course by numerous active faults (Burchfiel, Deng,

Molnar, & Wang, 1989; Burchfiel, Zhang, Wang, & Molnar, 1991; Gaudemer et al., 1995; Zhang, Mercier, & Vergdly, 1998).

The QGC is located in the boundary fault zone on the northeastern margin of the Qinghai–Tibetan Plateau, where active and neotectonic structures are clearly expressed. If the QGC is the product of tectonic activity, then it is plausible that paleo-river channels are preserved in the vicinity. We used remote sensing, shallow seismic profiling, shallow coring, and river terrace geomorphology to explore this possibility and assess the existence of relict river channel diversions in the Qingtongxia area. Such information is key to establishing the formation and evolution of the canyon and surrounding area.

2 | GEOLOGIC SETTING

Qingtongxia City is located in the central Ningxia Hui Autonomous Region of North China. Geologically, the area lies within a deformation belt formed by the intersection of the Qinghai–Tibetan Plateau to the west and the Ordos Block to the east (Zhou, 1985, 1994; Tapponnier, 1986; Deng, Cheng, Ma, & Du, 2014) and is bounded by the Yinchuan Basin to the north and Niushou Mountain to the south. The principal mountain block is the north–south-oriented Niushou Mountain, with an accumulation of extensive alluvial and diluvial fans around its base. The dominant landforms along the Yellow River in the Qingtongxia area are river platforms and terraces.

The main geologic units in the Qingtongxia area include the Ordovician Miboshan Formation ($O_{1-2}mb$), Paleogene Qingshuiying Formation (E_3q), Neogene Zhang'enbao (N_1z) and Ganhegou (N_2g) formations, and overlying Quaternary sediments (Huo, Pan, & You, 1989; Zhang et al., 2004b; Wang, Zhang, & Lei, 2013; Geological Survey Institute of Ningxia Hui Autonomous Regio, 2018; Liu, Hu et al., 2019; Liu, Shi et al., 2019 Figure 1). The Ordovician Miboshan Formation comprises medium-thickness layers of grey–green, fine- to medium-grained feldspathic quartzite sandstone, lithic quartz sandstone, slate, and conglomerate slate and is primarily exposed in the Niushou Mountain area (Zhang, Ma, Lei, & Ren, 2003). Lying unconformably atop the Ordovician (or older) strata and parallel to an unconformable contact with the Miocene Zhang'enbao Formation, the Paleogene Qingshuiying Formation consists of light purple–red, brick red, and orange–red mudstones, silty mudstone, and silty- to fine-grained sandstones, all of which are primarily exposed around Weiningbeishan and the western Niushou Mountain piedmont. The lower Neogene Zhang'enbao Formation comprises orange, clay-rich, sandy soil, and sandy clay, while the upper part of the unit consists of a pale red, sandy clay that crops out throughout Niushou Mountain. The Neogene Ganhegou Formation consists of orange–yellow conglomerate and sandstone that primarily occurs in the eastern Niushou Mountain piedmont, where only the lower strata of the group are exposed. The overlying Quaternary sediments are dominated by the calcareous conglomerates of the Yumen Formation (Q_1y), which exhibit an average thickness of 2 m. This lithology is composed of fine-grained grey, yellow–grey, and clay-red mega-conglomerate and arenaceous lenses. Middle Pleistocene alluvial fans are also well developed in the study area, as are grey gravels, sandy gravels, and khaki-coloured, gravelly silt–sand layers of Holocene age (Geological Survey Institute ofNingxia Hui Autonomous Regio, 2018).

Our study area is situated within the Niushou Mountain–Luoshan Fault Zone, at the outer margin of the northeastern Tibetan Plateau. Four secondary faults traverse the region: from west to east, they are the Qukou, Baima, Qingtongxia, and Kushuihe faults (Chen, Hu, Gong, Kang, & Li, 2015; Figure 1). The 40-km-long, NNE–SSW-trending Qukou Fault (F1) developed on the west bank of the Yellow River, between Hongshidun and Zaoyuanpu. The fault primarily exhibited N–S-oriented sinistral thrusting and an E–W-oriented right strike in its early stage, whereas the structure then evolved into a group of NNE–SSW- and NE–SW-trending conjugate normal faults. The Baima Fault (F2) developed in the western Niushou Mountain piedmont, extending 50 km from the head of Qingtongxia to Hongliugou. The principal structural features of F2 include dextral strike-slip shear and NE–SW-oriented strike-normal faulting in its late stage. The Qingtongxia Fault (F3) developed on the eastern side of Niushou Mountain as a NW–SE-striking dextral strike-slip fault; the Gezishan Fault extends for ~80 km on the northwestern side of F3 and lateral row with Luoshan Fault to the sout. The Luoshan Fault showed a group of conjugate strike-slip faults in the early stage followed with a N–S strike normal fault. The Kushuihe Fault (F4) is located on the west side of the Kushuihe River and exhibits a clear NW–SE-striking fault scarp. F4 was a sinistral strike-slip fault in its early stage, transitioning into a normal fault in its late stage (Chen et al., 2015; Gong et al., 2016).

The course of the Yellow River is highly complex from Baima to the exit of the QGC. The Yellow River flows 50 km to the north along the western Niushou Mountain piedmont from Baima. The Yellow River has incised a large Z-shaped bend into the hard Niushou Mountain sandstone at the head of the QGC as it flows northeast towards the Yinchuan Basin. During the early Pleistocene, the Yellow River was seized by tributaries draining the western Niushou Mountain piedmont; after which, the main channel was diverted towards the Yinchuan Basin (Liang et al., 2013). Pliocene tectonics also served to force the Yellow River northward into the Shapotou area (Zhang et al., 2004).

3 | IDENTIFICATION OF PALEO-RIVER CHANNELS

3.1 | Remote sensing interpretation

Despite widespread alteration of paleo-river channels by topographic change and human land use, these features are still identifiable via remote sensing. The primary indicator of paleo-river drainage is soil type due to the influence of river channels on the physical characteristics of soil. For example, relative differences in the spectra of the remotely sensed electromagnetic radiation emitted from soil surfaces have been employed as markers for identifying paleo-river channels (Carol, Braga, Donnici, Kruse, & Tosi, 2017). Here, we used Landsat Thermic Mapper (TM; Burgess, 1993; Wu, Leeuw, Skidmore, Prins, & Liu, 2007) and ASTER data (Ali, 2016; Poongodi & Venkateswaran, 2018) to interpret the geomorphological features, as both are sensitive to the water content characteristics of surface soils.

Ratio processing is commonly applied to TM data to highlight features with different slope values on the Popper curve. This is a highly effective way to extract the linear features of slowly changing transition zones, which typically lack significant topographical variations or sharp surficial colour contrasts. For example, minor variations in surficial spectral characteristics are caused by differences in soil water content, vegetation cover, microgeomorphology, geochemical reflection, and other surficial characteristics. Although water is a weak reflector in the TM2 wave band, it is ineffective in the TM5 band, such that TM5/2 can be used to extract information on the water content. Soils

that are devoid of water are typically characterized by pale shades of grey in remotely sensed images of paleo-river channels, whereas wetter areas return dark grey, blue, and black tones (Jessica, Shuhab, Mohamed, Abdel-Fattah, & Z., 2013).

ASTER imagery within the Yinchuan Basin reveals a N–S-trending feature along the west side of the Tanglai Canal, with the wet areas highlighted in black. Both the serpentine shape and banded form of this wet area suggest the existence of a paleo-river channel (Figures 2 and 3), while the southward extension of the channel and apparent connection with the modern river to the west of the Grand Canyon potentially delineate the former course of the Yellow River (Figures 2 and 3).

3.2 ⏐ Surface features

We conducted a field survey of the paleo-river channel site to verify our remote sensing-based interpretations. The modern land surface is characterized by wetlands, such as marshes and paddy fields, within the limits of the paleo-river channel, whereas the adjacent surfaces consist of dry land that is currently under corn cultivation (Figure 3 a). Compositionally, the paleo-river channel contains sorted gravels with well-rounded clasts of quartzite, metasilicate quartz sandstone, and granite, consistent with the bed load of the modern Yellow River. In contrast, the gravels exposed on either side of the paleo-river channel are neither sorted nor well-rounded, and primarily consist of sandstone and limestone that are potentially derived from local alluvial fan deposits.

An exposed unit of well-rounded Yellow River gravel can be seen overlying mudstones of the middle Miocene Zhang'enbao Formation

on the upper Qingtongxia platform (P50103; Figure 3b). A 20-m-thick sequence of sand and gravel layers is exposed at P50106 (Figure 3c) at the same height as P50103 but <50 m southeast. The imbrication of gravel clasts within this sequence is diagnostic of paleo-river flow in a south-to-north direction (Figure 3d). We also note the absence of faults between the two sets of strata, which we tentatively interpret as representing the estuarine position of the paleo-river channel flowing into the Yinchuan Basin.

3.3 ⏐ Land surface features

We also measured several land surfaces points along the northern part of the QGC. An exposure at point P50102 revealed an 80-cm-thick layer of medium-sorted gravel with subedge to subcircle roundness values. Although the gravel size decreases with height in this unit and the majority of clasts lie within the 1–2-cm range, we observed clasts as large as ~10 cm in diameter. A 50-cm-thick layer of loess caps the gravel unit (Figure 4a).

Two sedimentary units are exposed at point P50107. The upper stratum consists of moderately sorted grey gravel with medium- to fine-grained arenaceous lenses. The gravel clasts are 2–5 cm in diameter, exhibit medium roundness values, and are primarily composed of limestone and sandstone. The unit is characteristic of alluvial fan deposits. In contrast, the lower stratum is fluvial in nature and largely comprises sand and gravel layers (Figure 4b). Two sets of strata are exposed at point P50108. The upper unit is a 1.2-m-thick gravel layer with thick gravel interbeds that are characterized by fine sand lenses and is similar in appearance to an alluvial fan deposit. The lower unit consists of fine, grey-yellow sand layers that are characteristic of

FIGURE 3 Surficial geomorphology of the paleo-river channel. (a) Surface marsh environment at P50316; (b) Contact relationship between the Zhang'enbao Formation and Quaternary sediments; (c) Yellow River gravels overlying the Zhang'enbao Formation (N_1z); (d) P50106 Surficial gravel characteristics at P50106 [Colour figure can be viewed at wileyonlinelibrary.com]
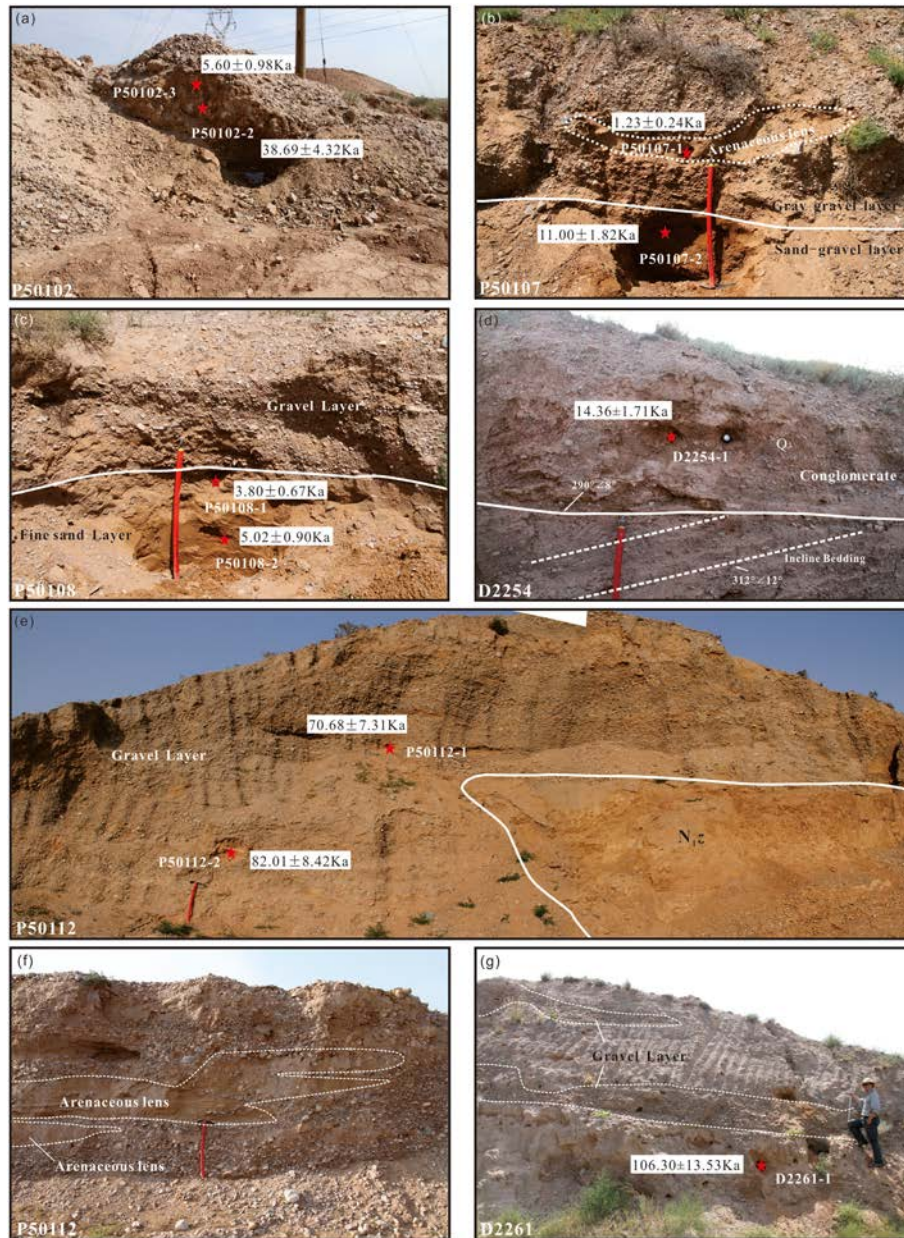
FIGURE 4 Characteristics of the paleo-river channel. (a) P50102 and the sampling position; (b) P50107 features and sampling position; (c) P50108 features and sampling position; (d) D2254 features and sampling positions; (e) P50112 features and sampling position; (f) P50112 gravel layer characteristics and sandy lens; (g) D2261 platform features and sampling position [Colour figure can be viewed at wileyonlinelibrary. com]

riverbed deposits (Figure 4c). An exposed sequence of poorly sorted, minimally rounded limestone gravel layers that are interbedded with arenaceous lenses and lack any fluvial facies is observed at point P50112, which is also suggestive of deposition on an alluvial fan (Figure 4e,f).

We documented gravel layers overlying a consolidated, grey-green gravelly sandstone at point D2254, with inclined bedding (presumably N$_2$g) that contained a consolidated conglomerate layer. The strata and inclined bedding are occurrence 290°∠8° and 312°∠12°, respectively and show a low degree of clast rounding, indicating that this basal unit corresponds to Q$_3$. In contrast, the upper part of the sequence comprises a grey-brown gravel layer with predominantly sandstone and

limestone clasts that exhibit moderate rounding and sorting, and staggered bedding is evident. These layers are interbedded with arenaceous lenses (Figure 4d). Finally, we observe a layer of poorly sorted, minimally rounded gravel that consists primarily of limestone and sandstone at point D2261 on the east side of the paleo-river channel, which we interpret as an alluvial fan deposit (Figure 4g).

3.4 | Shallow core characteristics

We extracted eight shallow cores from the paleo-river channel floor and adjacent areas to assess their internal characteristics (Figures 2

and 5). Since the surface of the water-rich areas has been covered by Holocene sediments, to observe whether there are deposits of the Yellow River below the Holocene, eight boreholes were designed to confirm the differences between the water-rich areas and both sides. The sites of the cores were designed in EW-trending profiles that cutting through the water-rich zones in the north, middle and south parts (Figure 2). Among them, ZK03 and ZK08 are formed the northern section, ZK02 and ZK07 are the central section. For the southern section, there are four shallow cores, which are ZK01, ZK04, ZK05, and ZK06, were laid in the conversion area between Yinchuan Basin and QGC because of the complex geomorphologic characters (Figure 2). Meanwhile, in order to compare the sediment difference between the water-rich zone and its two sides, there are four boreholes laid in the wet area, and another four boreholes were laid on both sides of the water-rich zone (Figure 2). In the field, the boreholes were placed on the ground surface were not obvious due to man-made modifications and sediment cover.

The lithology of core ZK1 includes a red clay, red gravelly-sandy clay, red gravelly clay, and red gravelly coarse-fine sandy soil, all of Holocene age. The Holocene gravels in the lower part of the core are predominantly derived from limestone and sandstone, and exhibit a high degree of sorting and rounding. A layer of red mudstone occurs in the middle of this unit. These Holocene gravels unit covers on the red mudstone unit that belongs to the Neogene Zhang'enbao Formation (Figure 5).

The top of core ZK2 consists of a brownish yellow silty clay, with well-rounded gravels comprising sandstone, quartzite, and other clasts at 3.8-m depth. The unit thickness is ~4.1 m (Figure 5). The lithology of core ZK3, from top to bottom, consists of gravelly red coarse-grained sand, yellow clay, gravelly yellow fine-grained sand, poor-rounded gravel, and yellow clay. Gravelly sandy clay begins to appear at 20.5-m depth. The gravel in this 2.5-m-thick unit, which is derived from red mudstone, is generally well-rounded (Figure 5).

The upper section of core ZK4 is dominated by yellow argillaceous silt, the middle section by yellow clay, and the lower section by yellow silty mudstone (Figure 5). Core ZK5 comprises a yellow silty clay in its upper and middle sections and yellow mudstones in the lower section (Figure 5). The lithology of core ZK6, from top to bottom, consists of gravelly red silty–sandy clay of Holocene age, gravelly red fine-grained sand, and well-rounded, sorted gravel. Lithologically, these sandstone and quartzite gravels are similar to modern Yellow River sediments (Figure 5). Core ZK7 comprises yellow Holocene clay overlying well-rounded, quartzite, and sandstone gravels of Pleistocene age. (Figure 5). Core ZK8 comprises red silty Holocene clay, gravelly yellow clay, and coarse-grained sand interbedded with yellow clayey fine-grained sand (2:1 ratio). The basal section consists of a 2.2-m-thick layer of predominantly quartzite and limestone gravel and yellow silty clay (Figure 5).

Our shallow core analysis identified gravel layers in cores ZK2, ZK3, ZK6, and ZK7 that have similar physical characteristics to
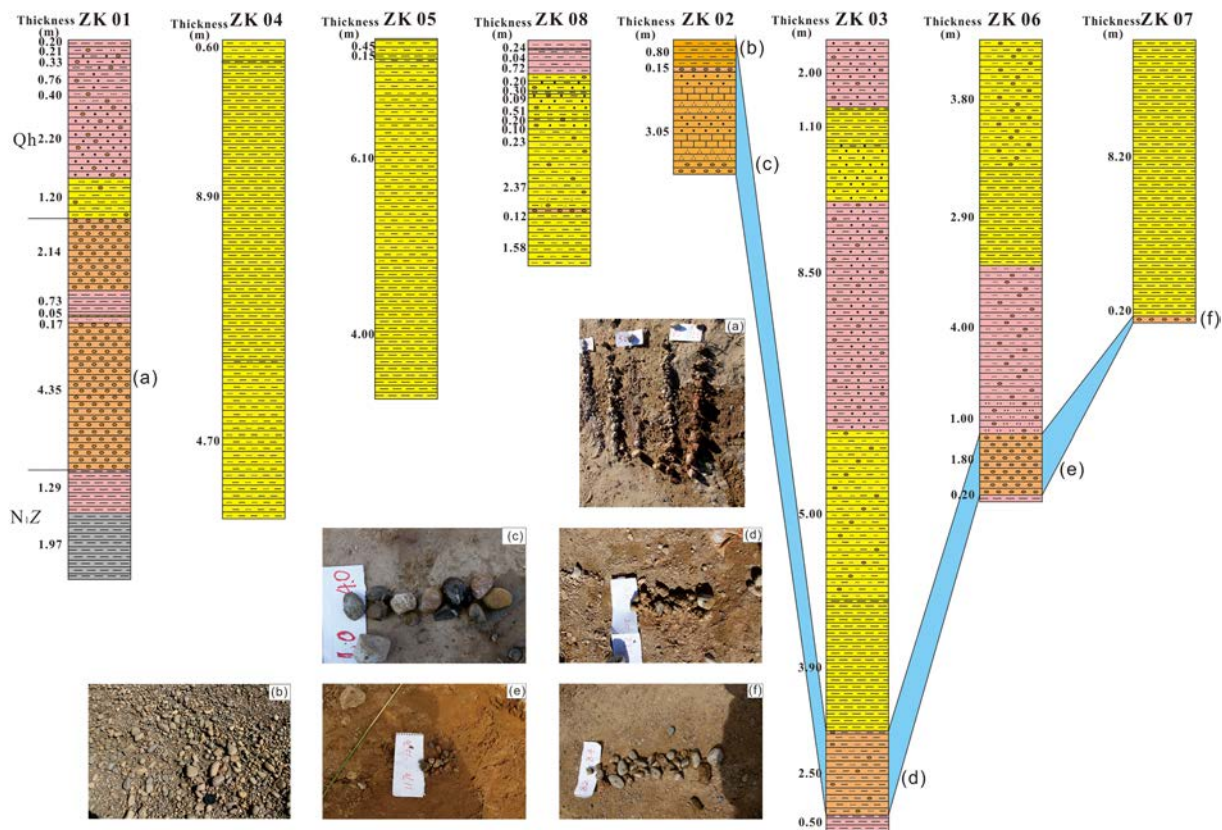
FIGURE 5 Shallow core cross-section. (a) ZK01, gravel at 8- to 12.5-m depth; (b) Surface gravel characteristics at ZK02; (c) ZK02 gravel characteristics at 1- to 4-m depth; (d) ZK03 gravel characteristics at 20- to 21.5-m depth; (e) ZK06 gravel characteristics at 11.7- to 12.7-m depth; (f) ZK07 gravel characteristics at 8.2- to 8.4-m depth [Colour figure can be viewed at wileyonlinelibrary.com]

contemporary Yellow River gravels. In contrast, Yellow River gravel was not recorded in cores ZK1, ZK4, ZK5, and ZK8, which were all collected from the land surfaces adjacent to the paleo-river channel. This pattern confirms that the paleo-Yellow River did not occupy those areas since they lack the diagnostic gravel deposits, thereby supporting the suitability of combined remote sensing interpretations and surface investigations for identifying paleo-river channels.

3.5 | Shallow seismic profile

We conducted a shallow seismic survey along National Road 109, in the southern section of the paleo river (starting point: 37°51′45.39″ N, 105°54′50.14″E; end point: 37°52′35.30″N, 105°55′07.98″E) to clarify the deep features of the paleo-river channel (Figure 2). The seismic profile imaged down to 1 km, providing a clear view of the deep structures in the study area (Figure 6). The seismic structures characterized by wavy lines in the eastern part of the profile are consistent with the strong fold and deformation of the Miboshan Formation strata in the Niushou Mountain area. In contrast, the western part of the profile is generally near-horizontal, consistent with the characteristics of the Cenozoic strata. A gentle west-sloping line between the two strata indicates the northward extension of the Baima Fault. Within the near-horizontal Cenozoic strata, there is a discontinuous belt located bellow the paleo-river channel we inferred in the seismic profile. This discontinuity can be interpreted as the normal faults same like to the Baima and Qukou faults (Figure 1).

4 | GEOMORPHOLOGICAL FEATURES OF THE YELLOW RIVER TERRACES

We investigated the geomorphology of the river terraces located at the entrance, central section, and exit of the QGC, in addition to the terraces near Baima in the upper reaches of the Yellow River. We measured the physical characteristics of terrace development for each landform in detail to produce four terrace sections: A–A′, B–B′, C–C ′, and D–D' (Figure 7).

4.1 | Sequence

Three terraces are observed at the exit of the QGC along terrace section A–A' (Figure 7), situated at 2, 10–15, and 25–31 m above the river (Table 1). Since the Qingtongxia Dam has raised the water level by ~14 m, this value must be added to the surface elevation of the terrace upstream of the dam to accurately correlate these features with terraces farther downstream. Gravel-dominated terrace T1 is visible on the west bank of the Yellow River, downstream of the dam, as shown in Figure 8. The river edge is submerged by the impounded Yellow River, and the terraces, partly obscured by marsh, are not immediately obvious upstream of the dam. Nonetheless, the T2 landforms are exposed on both sides of the Yellow River, located 1 and 10 m above the water line on the east and west banks, respectively (Figure 8), and both exhibit a clear dual structure and diagnostic Yellow River gravel composition. East of the Qingtongxia Dam, terrace T3 is situated 17 m above the water line, while this elevation difference is 25 m on the downstream west bank (Figure 8). The elevation of these terraces is essentially the same after considering the artificially high water-level upstream of the dam.

Nine terraces are preserved on the east bank of the Yellow River along central terrace section B–B′ (Figure 7). However, we observed no terrace features on the west bank, which is lithologically dominated by interbedded limestone (Ordovician Miboshan Formation) and sandstone. While T1 has likely been inundated in this section by the modern Yellow River (Figure 9), T2 is clearly exposed ~2 m above the water level (16-m predamming level), and T3 is situated at 32 m (Table 1). The above-ground scattered distribution of the Yellow River gravels on the terrace. We did not observe outcrops of the T4 terraces in this section (Figure 9), but T5 is evident at 34 m (Table 1), with accumulations of Yellow River sands and gravels derived from the mantle bedrock of the Miboshan Formation (Figure 9). T6 is situated 65 m above the river and possesses a thicker gravel layer (Table 1), while T7 (90 m above water level) contain an approximately 60-cm-thick gravel layer. And the gravel diameter is increasing eastward. The exposed gravel in the easternmost part of T7 has a consistent diameter of ~10 cm and no fine-grained component. The lower part of this
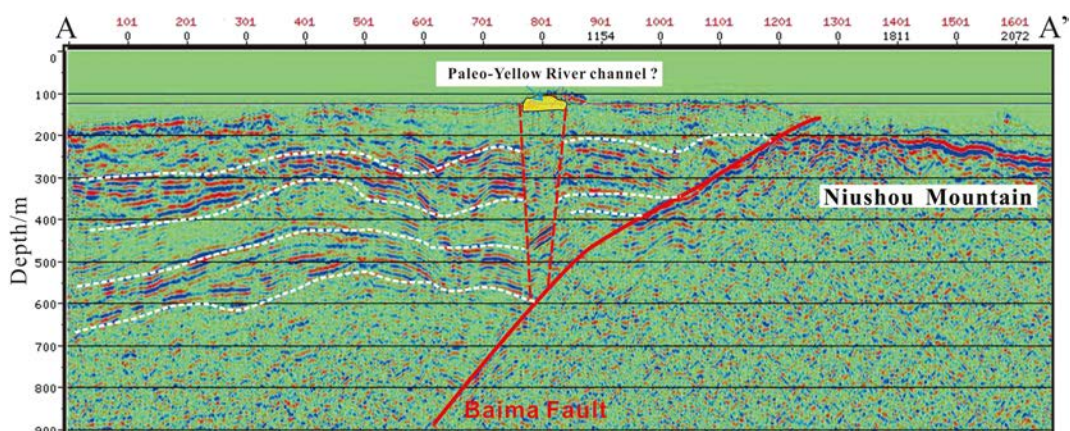
FIGURE 6 Interpretation of the shallow seismic profile depicting the paleo-Yellow River channel [Colour figure can be viewed at wileyonlinelibrary.com]
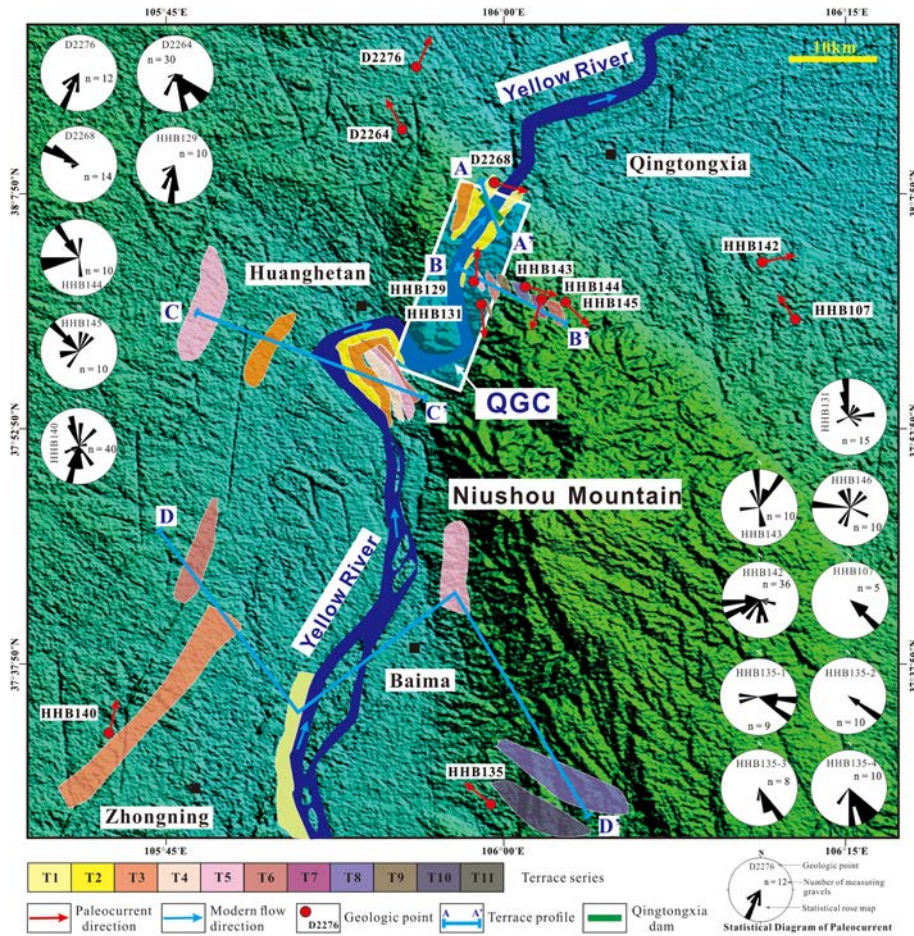
FIGURE 7 Distribution of the Yellow River terrace plane and its paleocurrent characteristics [Colour figure can be viewed at wileyonlinelibrary. com]

**TABLE 1** Comparison table of above water level in different terrace section

Terrance Number	Terrace section A–A	Terrace section B–B′	Terrace section C–C′	Terrace section D–D′
T1	2 m			1–3 m
T2	10–15 m	16 m	15 m	
T3	25–31 m	32 m	25–28 m	
T4			41 m	35 m
T5		48 m	54 m	57 m
T6		79–74 m	65 m	
T7		90 m		
T8		120 m		97 m
T9		124–129 m		
T10				
T11				164 m

gravel layer consists of maroon-coloured mudstone derived from the Ordovician Zhang'enbao Formation. T8, which is located 120 m above the modern river (Table 1), forms a hillock upon which well-rounded

and complex gravel layers of Yellow River provenance are abundant. The T5–T9 terrace is likely to be a deposit formed in the Pliocene.

The three terraces are also well developed in the central section of the QGC, consistent with the lower gorge observations. The older terraces are preserved farther from the modern river at higher elevations. The highest of these, T9, is located 124–129 m above the river (Table 1), and potentially corresponds to the paleo-river channel described above.

Five terraces are observed on the east side of the Yellow River at the head of the QGC along terrace section C–C′, of which T1 is presumed to have been submerged by the impounded river (Figure 7). Terraces T2–T5 are located at 15, 28, 41, and 54 m above the river (Table 1), respectively (Figure 10), with each exhibiting gravel and sandy soil layers, and clear binary structures. Terrace T6 is at 65 m and comprises little more than a scattering of gravel on the terrace surface. Terraces T3 and T5 are well preserved at 25 and 54 m actual height, respectively, on the west bank of the Yellow River, with the former corresponding to the early paleo-river channel. Terrace T5 is the most extensive terrace in the vicinity. The only remaining fragment of T2 is ~2 km south of the isthmus, ~8 m above the water level. We found there is no gravel or terrace topography higher than the T6 terrace in the western Niushou Mountain on the east bank of the
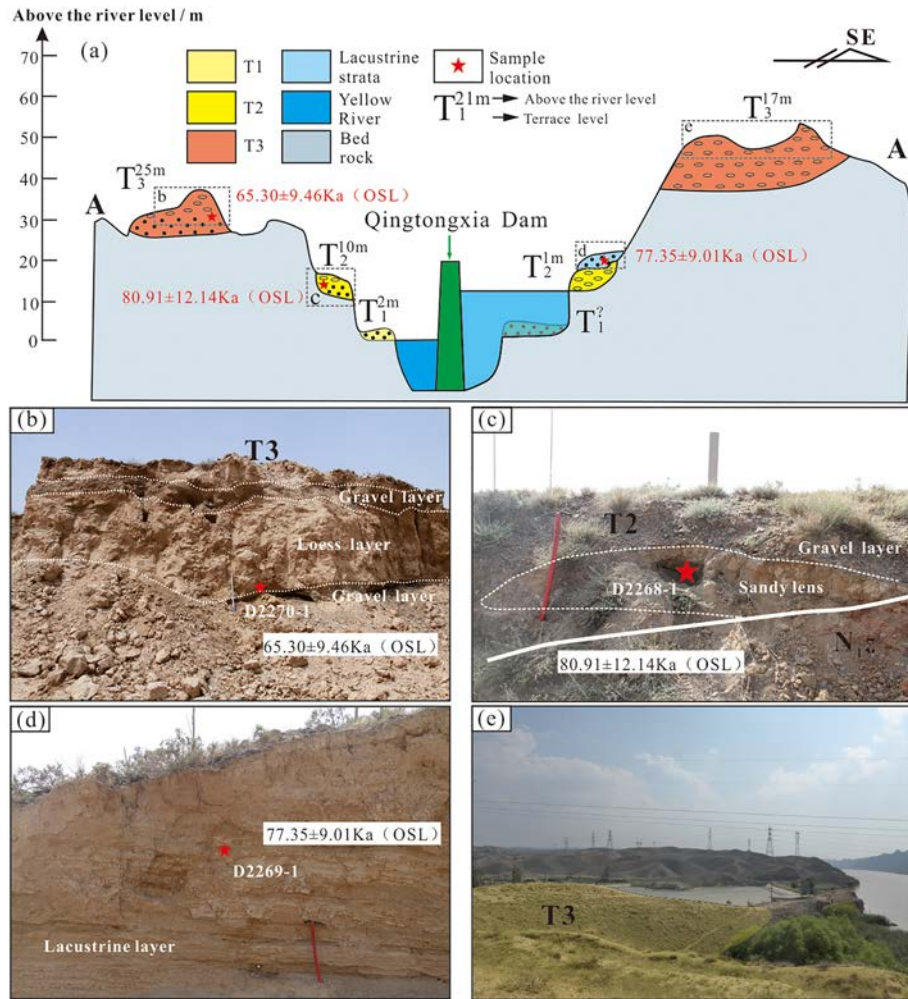
FIGURE 8 Lower terrace section A–A'. (a) Terrace section downstream of Qingtongxia Dam; (b) Terrace T3 features and sampling location on the west bank; (c) Terrace T2 features and sampling location on the west bank; (d) T2 overlying lacustrine strata on the east bank; (e) Macrofeatures of terrace T3 on the east bank [Colour figure can be viewed at wileyonlinelibrary.com]

Yellow River and the Weining North Mountain on the west bank, especially in the Weining North Mountain with smaller slope (Figure 10). The higher terraces in the western Yellow River area could not be eroded by the late tectonic activity or climate change, because the terrain changes very limited. So T6 should be the highest terrace in western Niushou Mountain area.

Six terraces are observed in the upper reaches of the Yellow River near Baima along terrace section D–D' (Figure 7). By measuring the modern water level, we established that the river surface elevation at Baima has increased significantly since construction of the Qingtongxia Dam, resulting in widespread submergence of terrace T1 in this area. Two terraces, T1 and T5, were identified on the west bank near Baima Township (Figure 11). While the front edge of T1 rises only a metre above the water level, its distal edge is located at 3 m and has become part of the river's flood plain (Table 1). The surface of T1 is characterized by a cover of fine sand and extensive vegetation. Terrace T5 is situated 57 m above water level (Table 1) and is demarcated by an accumulation of Yellow River sand and gravel. We identified the

remains of three terraces, T4, T8, and T11, on the east bank of the river (Figure 11). T4, which is comprised of Yellow River gravel, sits at 35 m above the river, while T8 and T11 are at 97 and 164 m (Table 1), respectively, is the Pliocene Ganhegou Formation.

4.2 | Paleocurrent flow

We conducted paleocurrent direction statistics for selected terraces to further establish the relationship between paleo-river channels and the flow directions recorded by relict river terraces. The paleo-flow direction of the Yellow River was roughly like the present conditions, as shown in Figure 12. South-to-north paleocurrent flow was determined near the Qingtongxia railway station (Figures 7, and 12a,c). However, the paleo-flow directions were more complex to the east of the QGC. For example, terraces T5–T9 indicate flow in a northwest-to-southeast direction (Figure 7), whereas terrace T3 in western Zhongning County depicts primarily south-to-north flow
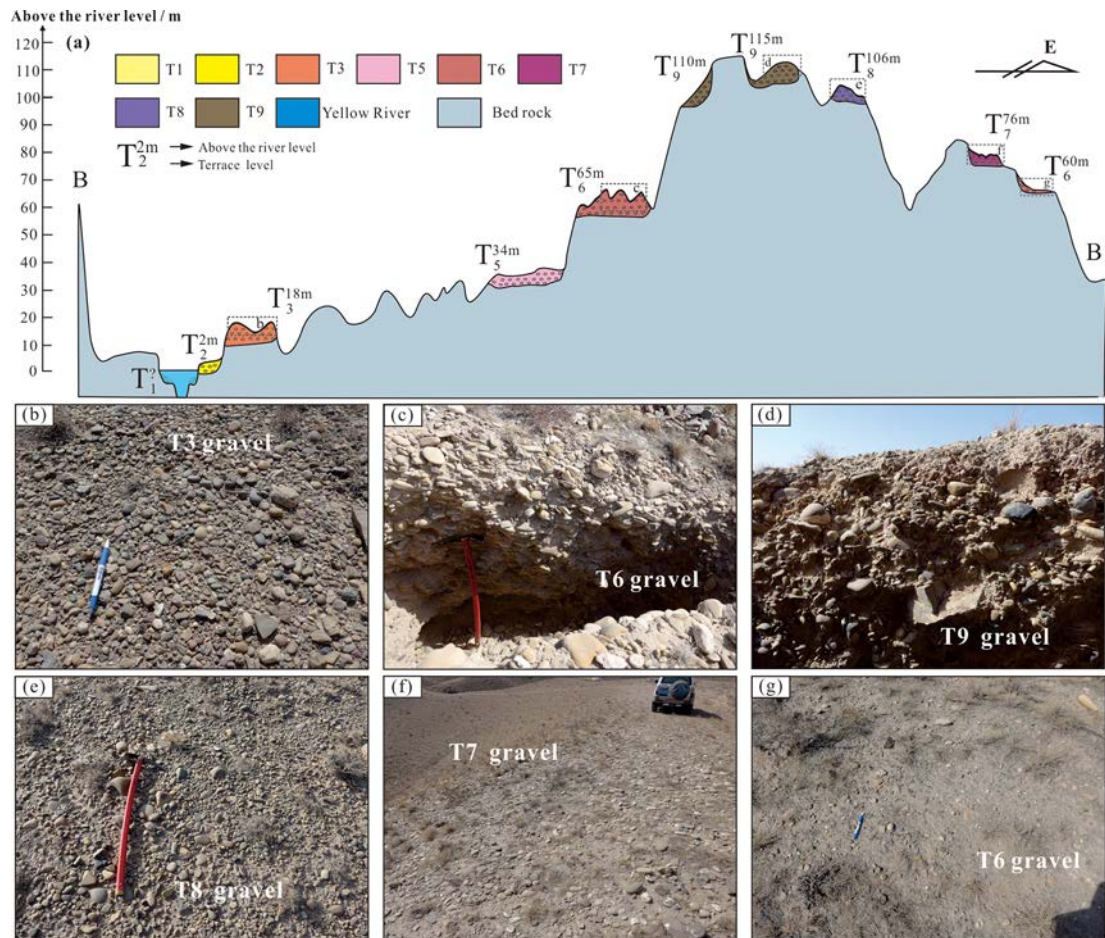
FIGURE 9 Central terrace section B–B′. (a) Profile of the Yellow River terraces in the central part of the QGC; (b) Characteristics of Yellow River gravel in terrace T3; (c) Yellow River gravel in terrace T6; (d) Yellow River gravel in terrace T9; (e) Characteristics of Yellow River gravel in terrace T8; (f) Terrace T7 features; (g) Terrace T6, which is comprised of Yellow River gravels [Colour figure can be viewed at wileyonlinelibrary.com]

(Figure 7 and 12b). A southeast-to-northwest paleocurrent direction is reconstructed from T8 near Baima (Figures 7 and 12d). According to our statistical treatment of these data, we posit that the Yellow River flowed through the eastern piedmont of Niushou Mountain during the Neogene development of the Ganhegou Formation. Thereafter, flow was redirected along the western Niushou Mountain piedmont, resulting in an essentially south-to-north flow direction that continues today.

5 | CHRONOLOGY RESULTS

Previous studies have identified the Yellow River terraces as primarily Pleistocene in age (Hu et al., 2017; Pan et al., 2005, 2012). We applied optically stimulated luminescence (OSL) dating to define the timing of terrace development and constrain the fluvial chronology in more detail. OSL analyses were conducted at the Key Laboratory of Crustal Dynamics, Institute of Crustal Dynamics, China Earthquake Administration, using the sensitivity-corrected multiple aliquot regenerative-dose and single-aliquot regenerative-dose methods.

This study shows that the QGC was incised after the first phase of the Yellow River channel change, with the outlet developing low-level

terraces during this time. We collected samples for OSL dating from the terrace profile located at the entering of the Qingtongxia gorge to determine exactly when the canyon incision occurred. For T2, we calculated ages of 80.91 ± 12.14 ka for the west bank terrace and 77.35 ± 9.01 ka for the lacustrine strata atop the east bank terrace (Table 2). A third age, 65.30 ± 9.46 ka, was returned from terrace T3 on the west bank (Table 2). Based on these results, we infer that the QGC formed at 65–80 ka, concurrent with the Yellow River channel shift.

The spatial distribution of terraces T2 and T3 at the head of the QGC is consistent with the current river channel, indicating that these are modern river terraces. In contrast, the distribution of terraces T4–T6 aligns more closely with the paleo-river channel identified via remote sensing and is therefore considered to correlate with that drainage pattern. We collected OSL samples from two sites on terrace T3. The ages from point D2266 are 52.89 ± 7.65 ka and 86.14 ± 11.12 ka (Table 2), while those from point D2260 are 69.54 ± 7.47 ka and 96.52 ± 13.89 ka (Table 2). Both sets of ages are similar to those from entering of the canyon, further supporting the formation of the QGC at ~85 ka. A single OSL sample from terrace T2 at this site returned an age of 11.49 ± 1.47 ka (Table 2).
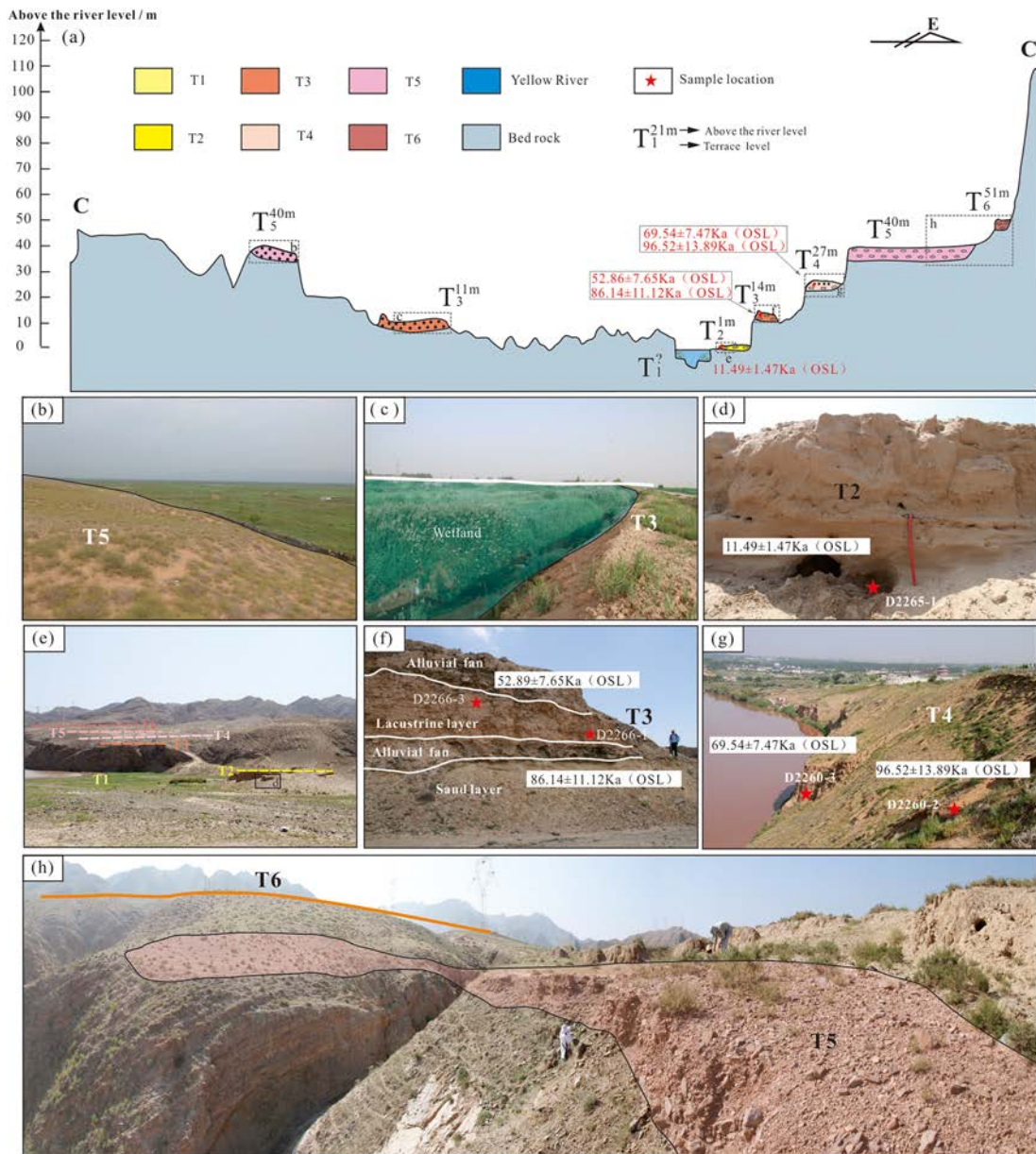
FIGURE 10 Upper terrace section C–C′. (a) Profile of the Yellow River terraces at the entrance to the QGC; (b) Macroscopic characteristics of terrace T5 on the west bank; (c) T3 terrace features on the west bank; (d) T2 terrace features and sampling location on the east bank; (e) Macroscopic features of the east bank terrace; (f) Macroscopic features of the east bank [Colour figure can be viewed at wileyonlinelibrary.com]

Several OSL ages constrain the timing of incision of the northern Great Bend. The upper gravel layer at P50102 gave an age of 5.60 ± 9.8 ka, and a lower unit gave an age of 38.69 ± 4.32 ka (Table 2, Figure 4a), indicating that the Yellow River was diverted from its former channel after ~39 ka. A sample collected from the upper alluvial fan at point P50107 (Figure 4b) returned an age of 1.23 ± 0.24 ka (Table 2), while a sample from the underlying layer of fluvial sand dates to 11.0 ± 1.82 ka (Table 2), suggesting that the Yellow River was still occupying the relict channel at that time. Similarly, two OSL ages on the lower stream sediments exposed at P50108 indicate channel occupation between 3.80 ± 0.67 ka and 5.02 ± 0.9 ka (Table 2, Figure 4c). These data lead us to speculate that, even after

the main channel of the Yellow River had abandoned this paleo-river channel in favour of a new route through the QGC, minor tributaries continued to deposit sediments in the now-relict channel. Two ages from the alluvial fan at P50112 (Figure 4e) are, in order of increasing depth, 70.68 ± 7.31 ka and 82.01 ± 8.42 ka (Table 2), confirming that the Yellow River did not pass through the site after ~82 ka. Finally, a single age of 14.36 ± 1.71 ka from the alluvial fan at point D2254 (Table 2, Figure 4g) provides a minimum age for the abandonment of that site by the Yellow River.

The highest Yellow River terrace, T11, is located near the Baima Township and comprises a consolidated gravel layer associated with the Neogene Ganhegou Formation. This unit belongs to fluvial facies
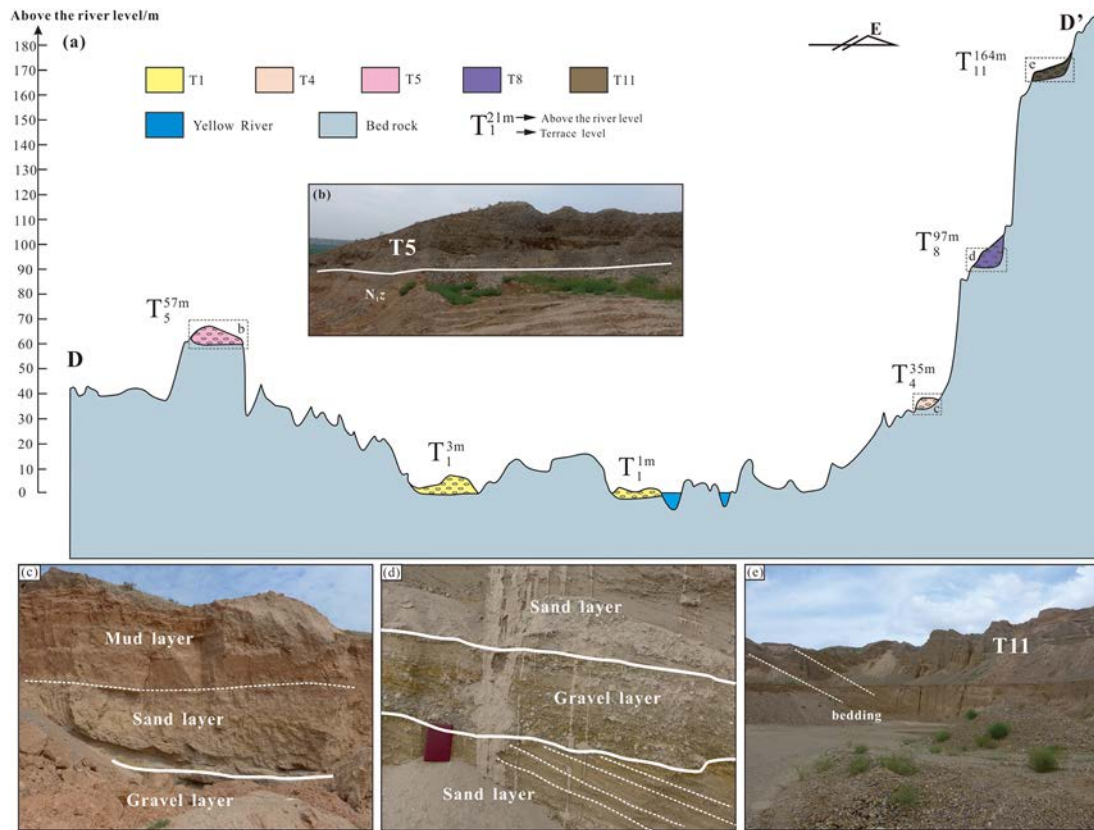
FIGURE 11 Baima terrace section D–D', near the paleo-river channel. (a) Profile of the Yellow River terraces at Baima; (b) Terrace T5 characteristics on the east bank; (c) Terrace T4 features on the east bank; (d) Terrace T8 features on the east bank; (e) Terrace T11 features on the east bank [Colour figure can be viewed at wileyonlinelibrary.com]
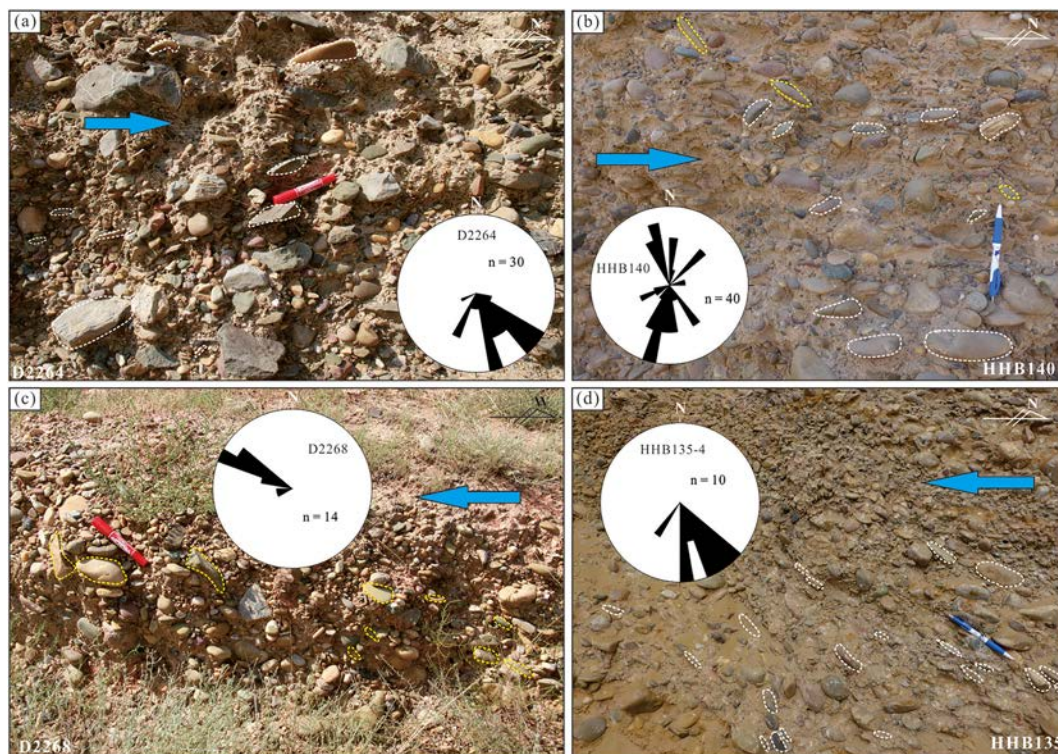
FIGURE 12 Characteristics of the gravel arrangements in the Yellow River terraces. Flat surface gravel characteristics and paleocurrent statistics for (a) Point D2264, (b) Point HHB140, (c) Point D2268, and (d) Point HHB135 [Colour figure can be viewed at wileyonlinelibrary.com]

TABLE 2 Optically stimulated luminescence age results in Qingtongxia area.

Sample Number	Location	U (μg/g)	Th (μg/g)	K (%)	Environmental Dose Rate (Gy/ka)	Grain Size (μm)	Method	Equivalent Dose (Gy)	Age (ka)	above the water level	Terrace level	Reliability
D2254-1	N37°52′06.64″ E105°56′20.52″,H:1,195 m	1.61	5.48	1.35	2.70	4–11	SMAR	38.77 ± 2.51	14.36 ± 1.71	55 m		Trustworthy
D2260-2	N37°50′07.69″ E105°57′05.78″, H:1,165 m	1.68	6.98	1.63	3.17	4–11	SMAR	306.08 ± 31.65	96.52 ± 13.89	25 m	T3	Trustworthy
D2260-3	N37°50′07.69″ E105°57′05.78″, H:1,165 m	1.42	5.28	1.74	3.01	4–11	SMAR	209.57 ± 8.23	69.54 ± 7.47	25 m	T3	Trustworthy
D2261-1	N37°51′13.62″ E105°57′00.81″, H:1,195 m	3.10	7.64	1.69	3.82	4–11	SMAR	405.98 ± 31.95	106.30 ± 13.53	55 m		Trustworthy
D2265-1	N37°49′03.10″ E105°57′24.49″, H:1,161 m	1.87	9.65	1.59	3.48	4–11	SMAR	39.96 ± 3.21	11.49 ± 1.47	21 m	T2	Trustworthy
D2266-1	N37°47′51.17″ E105°57′15.37″, H:1,164 m	1.79	8.59	1.60	3.35	4–11	SMAR	288.32 ± 23.55	86.14 ± 11.12	24 m	T3	Trustworthy
D2266-3	N37°47′51.17″ E105°57′15.37″, H:1,164 m	2.51	10.20	1.93	4.12	4–11	SMAR	217.80 ± 22.75	52.89 ± 7.65	24 m	T3	Trustworthy
D2268-1	N37°52′47.14″ E105°59′24.46″, H:1,160 m	1.79	7.02	1.65	3.24	4–11	SMAR	261.84 ± 29.28	80.91 ± 12.14	20 m	T2	Trustworthy
D2269-1	N37°52′46.63″ E105°59′34.90″, H:1,154 m	1.75	7.48	1.78	3.40	4–11	SMAR	263.29 ± 15.73	77.35 ± 9.01	14 m	T2	Trustworthy
D2270-1	N37°53′31.98″ E105°58′57.82″, H:1,165 m	3.13	9.79	1.87	4.24	4–11	SMAR	276.85 ± 29.04	65.30 ± 9.46	25 m	T3	Untrustworthy
P50102-2	N37°55′21.43″ E105°56′17.54″, H:1,163 m	2.51	11.7	1.37	2.90	90–150	SAR	112.14 ± 0.58	38.69 ± 4.32	23 m		Trustworthy
P50102-3	N37°55′21.43″ E105°56′17.54″, H:1,163 m	2.46	10.8	1.42	2.87	90–150	SAR	16.07 ± 2.31	5.60 ± 0.98	23 m		Trustworthy
P50107-1	N37°56′07.34″ E105°57′0.46″, H:1,146 m	1.47	7.38	1.26	2.23	90–150	SAR	2.75 ± 0.46	1.23 ± 0.24	6 m		Trustworthy
P50107-2	N37°56′07.34″ E105°57′0.46″, H:1,146 m	1.68	6.33	1.17	2.12	90–150	SAR	23.33 ± 3.08	11.00 ± 1.82	6 m		Trustworthy
P50108-1	N37°56′18.54″ E105°56′54.91″, H:1,148 m	1.80	6.06	1.14	2.11	90–150	SAR	8.01 ± 1.15	3.80 ± 0.67	8 m		Trustworthy
P50108-2	N37°56′18.54″ E105°56′54.91″, H:1,148 m	1.66	7.56	1.31	2.34	90–150	SAR	11.76 ± 1.75	5.02 ± 0.90	8 m		Trustworthy
P50112-1	N37°57′06.09″ E105°56′32.00″, H:1,163 m	1.26	4.41	0.83	1.56	90–150	SAR	110.56 ± 2.89	70.68 ± 7.31	23 m		Trustworthy
P50112-2	N37°57′06.09″ E105°56′32.00″, H:1,163 m	1.06	3.81	1.09	1.72	90–150	SAR	141.05 ± 3.25	82.01 ± 8.42	23 m		Trustworthy

Note. Samples were tested in the Key Laboratory of Crustal Dynamics, Institute of Crustal Dynamics, China Earthquake Administration. Samples were measured using sensitivity-corrected multiple aliquot regenerative-dose and single-aliquot regenerative-dose methods to obtain equivalent metrological values; after which, the growth curve was fitted via the saturation index method. It was shown that the regeneration dose point of fine particle samples measured via the simple multislice method was not well dispersed, and the growth curves of the other samples were not saturated, with the exception of sample D2270–1. We consider the test data for this batch to be reliable.

that is representative of the paleo-river channel of the Yellow River (Liang et al., 2013; Regional Geological SurveyInstitute of Ningxia Hui Autonomous Regio, 2018); the lowermost terrace of which is T8.

6 | DISCUSSION

6.1 | Evidence of the existence of paleo-rivers channels

We have applied a combination of remote sensing, surface investigations, shallow cores, and shallow seismic profiling to confirm the existence of the paleo-Yellow River channel at the QGC. TM5/2 and ASTER imagery revealed a N–S-oriented black strip that is indicative of saturated soil conditions, while subsequent surficial and shallow core analyses established that the surface of the paleo-river channel is characterized by wetlands today. The formation of marshes represents an environment in which the river, oxbow lake, or floodwater washout was passed in the early years (Knight & Kadlec, 2000; Yin, Qin, Liu, & Qiu, 2006). If it is the cause of the flood, the surface of the water-rich zone will be poor of grinding circle gravels and bad sorting. However, based on the field investigation, we found that the gravel layer in the water-rich zone is typical Yellow River gravel (Figures 3 and 5). The physical characteristics of the surficial and subsurface gravels analysed here, in addition to the data reported in previous studies, describe well-rounded, sorted sediments that are diagnostic of the Yellow River (Xing et al., 2002; Liu et al., 2003; Zhang et al., 2004; Pan, Liu, Gao, Wang, & Li, 2007; Fu, Zhang, Ma, Wang, & Wu, 2013; Hu et al., 2019). And some gravels, which are like these features of the Yellow River, are exposed throughout the region. It is widely believed that these gravel layers correspond to Yellow River gravel. In contrast, surficial and subsurface sediments on either side of the paleo-river channel are dominated by poorly sorted, minimally rounded gravels of alluvial and diluvial origin (e.g., ZK1 and ZK8). So the wet area or soil water content is considered that the Yellow River ancient river course is more likely.

Stark differences in the seismic structure between the paleo-river channels and their former banks have been attributed to fault activity (Feng et al., 2011), reflection of the river channel, or the river channels past the fault surfaces that existed before (Kong et al., 2016; Kou & Du, 1995; Liu et al., 2018). A very deep effect can be observed from the shallow seismic profile, but the effect of the river course on the seismic profile will not be so great. It is very likely that the early faulting activity formed a fault depression belt. Then, the Yellow River eroded along the subsidence area to form a channel, indirectly proving the existence of ancient rivers. Through remote sensing, seismic imaging, surface investigations, and shallow coring, we have demonstrated the existence of a paleo-Yellow River channel to the north of the QGC. Furthermore, our surface investigation delineates the estuarine transition of this paleo-river channel into the Yinchuan Basin (P50106).

6.2 | Development of the Yellow River terrace in Qingtongxia

Based on our study of terrace landforms, paleocurrents, and chronology in the Qingtongxia area, we infer that three principal terraces are preserved at the exit of the QGC, eight terraces in the central section of the gorge (of which T9 is the highest and T4 is absent), and six terraces at the entrance. We also identified five terrace levels in the Baima Township. Through field investigation of the three sections, no higher terraces were found. So, the highest terrace at the exit of QGC is considered to be T3, the highest terrace in the middle of QGC is T9, the highest terrace in the entrance of QGC is T6, and the highest terrace in Baima Township is T11. Previous work reported seven terraces at Xueying, in the southern reaches of the Baima Township, and six terraces near Wudachang (Liang et al., 2013), where the superlative terrace was consistent in height with T7 in the central section of the QGC.

The distribution of terraces T4 and T5 along the Yellow River near Baima correspond to the advanced terraces at the head of the QGC, whereas the higher terraces in this area correlate with the paleo-river channel. By comparing the upper and lower Yellow River terraces in Qingtongxia, it is evident that the terraces of upper reaches are clearly more series than the lower, suggesting that the upper terraces predate the lower landforms. An advanced terrace situated above the level of T8 in the southern reaches of the Baima Township is in contrast to the situation north of Baima Township, where the uppermost terrace is represented by T6. Nonetheless, a similar high-level terrace is also preserved above T8 in the southern and eastern Niushou Mountain piedmont, indicating that the Yellow River likely flowed to the south of Niushou Mountain prior to the development of terrace T8.

We show that the Yellow River flowed into the Yinchuan Basin along the eastern Niushou Mountain piedmont, in agreement with the findings of an earlier investigation of sedimentary facies characteristics (Liang et al., 2013). The Pliocene Ganhegou Formation remains in the west side of the Baima Fault may also be a channel of the old Yellow River. Because the Ganhegou Formation in the west side of the Baima Fault has only a small part of the stratum. The horizontal displacement of the Ganhegou Formation on the east and west sides of the Baima Fault is about 10 km, which may be related to the dextral strike-slip deforamtion of the Baima Fault (Chen et al., 2015; Liang et al., 2013). Therefore, it is considered that the formation of Ganhegou Formation is caused by the fault of the late strike-slip, and the possibility of the branch of the ancient Yellow River channel is less.

The advanced terrace in the middle of the Qingtongxia Grand Canyon has not been determined at present, and it is considered to Ganhegou Formation, because the height of above the river is higher than the Ganhegou Formation deposit at east (Figure 9).

Four terraces are preserved in the Shapotou area in the upper reaches of our study, the highest of which is situated 200 m above the water level (Yan & Dong, 1997). Elsewhere, a total of 14 terraces were identified in the Mijiashan area, with the highest terrace situated at 377 m (Su, Ren, Zhang, Zhang, & Pichawut, 2019). A total of 10 terraces were reported from the Heishanxia area, the highest of which

was situated at 247 m, with cosmogenic nuclide dating placing deposition at 2.4 Ma (Zhang et al., 2004). Three terraces were found in the Sanmenxia area, and the highest terrace was 30–35 m in height of above the water level, the age of magnetic stratigraphy is 1.165 Ma (Pan et al., 2005). The uppermost terrace in the Shanxi–Shaanxi gorge area is analysed with the magneto-stratigraphy study; its age is 3.7 Ma (Pan et al., 2012). Five levels of Yellow River terraces in the Sanmenxia region area were dated, and the ages from T5 to T1 were 1.24 Ma, 0.86 Ma, 0.62 Ma, 129 Ka, and 12 Ka, respectively (Hu et al., 2017). Both the respective heights above water level and ages of these terraces are significantly greater than those reported in our study, suggesting that the Yellow River did not pass through the Qingtongxia area in the early stages, and the Yellow River's developmental period is at least 2.4–3.7 Ma.

Our study demonstrates that only low-elevation terraces are preserved at the exit of the QGC and that the extension of the lowest terrace at the canyon head is consistent with the modern Yellow River. Similarly, the paleocurrent flow direction is in accordance with the current flow direction. Throughout the study areas, higher terraces and paleocurrent directions exhibit a broad north-to-south alignment, consistent with the orientation of the paleo-river channel identified using remote sensing. We speculate that development of the bend occurred after the deposition of terrace T3 based on our analysis of the distribution characteristics of the Qingtongxia terraces. These results indicate that the QGC was rerouted prior to development of terrace T3 at ~85 ka and that the Yellow River followed this new route into the Yinchuan Basin during the late Pleistocene.

There was intense tectonic activity in the study area during this time, resulting in the formation of four active faults in the Yinchuan Basin, north of Niushou Mountain. The Helanshan Piedmont (Deng et al., 1985; Liu et al., 2017) and Yellow River faults, for example, have both exhibited periodic tectonic activity since the formation of the Yinchuan Basin. The active period of the Yellow River Fault, which transitioned from thrust to normal faulting in the late Pleistocene (Bao, Chen, Hu, & Zhu, 2019), is ~3,000 years. Concurrently, the Gezishan Fault in northwest Niushou Mountain switched from SW–NE thrusting to sinistral strike-slip thrusting (Gong et al., 2016), indicating intense late Pleistocene tectonic activity in the study area, which raises the possibility that changes in river channel flow were related to regional tectonic activity.

Normal fluvial sediments are 30- to 50-m thick, while the Yellow River sediments are 100 m in thickness. This suggest the Pliocene Ganhegou Formation was originally a subsidence area, which may be a part of the Yinchuan Basin (Liu et al, 2019). In the Late Miocene–Pliocene, due to the strong compression of the northeastern margin of the Tibetan Plateau, the ancient Yellow River channel, which developed in the east area of Niushou Mountain, was transformed from a fault depression to compression depression area (Zhou, Wang, & Cao, 1985; Zhou et al., 1994; Tapponnier, 1986; Zhang et al., 1988; Deng et al., 2014; Liu et al, 2019). This changing maybe causes the thickness of Ganhegou Formation to be so thick. Similar to the Yellow River in the Hetao Basin, thick Yellow River sediments have developed due to the Yellow Rivers location in the subsidence area (Zhao, Jia, & Hu, 2018).

6.3 | Changes in the paleo-Yellow River channel in Qingtongxia

Previous work in Qingtongxia and upper reaches area provided important baseline information on the fluvial evolution of the Yellow River (Zhang et al., 2004a; Liang et al., 2013). The middle-late Pleistocene Yellow River migrated from the Yongkang–Nanzhuang–Changle region of southern Zhongwei County to the Diaopoliang region of northern Zhongwei County based on drilling observations and surface geomorphology (Zhang et al., 2004b). Similarly, prior to the Pliocene, the river passed through the southern Niushou Mountain before draining into the Yinchuan Basin via the eastern Niushou Mountain piedmont (Liang et al., 2013).

We found that the distribution of terrace morphologies predating terrace T8 near Baima does not correspond to the modern flow direction of the Yellow River, but instead describes an east-to-west flow direction that is indicative of the river passing south of Niushou Mountain. Furthermore, pre-Pliocene terraces in northern Niushou Mountain tentatively indicate a northwest-to-southeast flow direction at that time (Figure 12). We suggest this pattern corresponds to one of two possibilities during the Pliocene: (a) The Yellow River, except along the eastern Niushou Mountain piedmont, had a tributary that flowed northward along the western Niushou Mountain piedmont and then southward along the northern part of Niushou Mountain, joining with the main Yellow River channel at that time; (b) The Yellow River was joined at Qingtongxia by a northwest-to-southeast flowing tributary that drained northwestern Niushou Mountain.

The residual sediments associated with these relict terraces/river channels should be preserved above the level of T8 in the western Niushou Mountain piedmont if the first hypothesis holds. However, the highest terrace in this area is T6, and no earlier landforms or paleo-Yellow River sediments have been identified to date, leading us to suggest this model is unlikely. There must also be residual high-grade terraces or stranded Yellow River sediments preserved in northwestern Niushou Mountain for the second hypothesis to hold. According to published data and field investigations (Geological Survey Institute of Ningxia HuiAutonomous Regio, 2018), it is apparent that the fluvial facies of the Ganhegou Formation are indeed exposed on the eastern and western sides of the Weiningbeishan and Helanshan areas. Therefore, the second hypothesis is more likely to be correct.

The Pliocene Yellow River flowed north along the eastern Niushou Mountain piedmont and drained into the Yinchuan Basin after the confluence with a tributary of the northwest stream in the Qingtongxia area (Figure 13a). Intense tectonic activity along the northeastern margin of the Qinghai–Tibet Plateau during the early-middle Pleistocene (Deng et al., 2014; Molnar & Tapponnier, 1975; Shi et al., 2015; Tapponnier, 1986; Zhang et al., 1988; Zhou et al., 1985; Zhou et al., 1994) resulted in faulting at Baima that influenced the location of the paleo-Yellow River channel. Specifically, the main river channel was diverted north along the western Niushou Mountain piedmont, whereupon the branch flowing through northwest Niushou Mountain was depleted (Figure 13b).

FIGURE 13 Evolution of the Yellow River in Qingtongxia area since the Pliocene [Colour figure can be viewed at wileyonlinelibrary.com]

However, the QGC did not form at this time. Based on our identification of a paleo-river channel to the north of the head of the canyon, we propose that although the Yellow River continued to flow along the western Niushou Mountain piedmont during the early Pleistocene, it did not do so via the QGC. Instead, the Yellow River switched its channel configuration during the early-middle Pleistocene. Our terrace physiognomy, paleocurrent direction, and chronologic data show that the northern channel at the QGC was abandoned due to tectonic activity at 65–85 ka, during which time the Yellow River was diverted through the QGC towards the Yinchuan Basin (Figure 13c).

7 | CONCLUSIONS

1. We analysed remote sensing imagery, surface geomorphology, shallow cores, and a shallow seismic profile to establish the existence of a paleo-river channel that extends north from the QGC.

2. The physical characteristics of the relict river terraces exhibit clear differences between the upper and lower reaches of the QGC. Only terrace T3 (25–27 m above water level) is preserved at the exit of the canyon, whereas terrace T6 (63 m above water level) located at the head of the canyon. The switch in flow direction from southwest to northeast indicates that the Yellow River changed its channel twice in the Qingtongxia area, first prior to development of T8 and again prior to T3.

3. Chronological data constrain the timing of incision of the QGC to 65–85 ka, which we take as evidence for the Yellow River shifting channels during the late Pleistocene.

CONFLICT OF INTEREST

No conflict of interest exits in the submission of this manuscript, and manuscript is approved by all authors for publication.

ORCID

Hong Chen https://orcid.org/0000-0002-6081-9232
Wei Shi https://orcid.org/0000-0003-1452-1555

REFERENCES

Ali, C. D. (2016). Flood hazard vulnerability for settlements of Turkey's province of Edirne, using ASTER DEM data and Landsat-7 ETM+ image data. *Arabian Journal of Geosciences*, *9*, 189.

Bao, G. D., Chen, H., Hu, J. M., & Zhu, G. F. (2019). Quaternary activity and segmentation of the Yellow River fault of the eastern margin of Yinchuan Graben. *Acta Geoscientica Sinica*, *40*(4), 614–628. (in Chinese with English abstract)

Burchfiel, B. C., Deng, Q. D., Molnar, P., & Wang, Y. P. (1989). Intracrustal detachment within zones of continental deformation. *Geology*, *17*(8), 748–752.

Burchfiel, B. C., Zhang, P. Z., Wang, Y. P., & Molnar, P. (1991). Geology of the Haiyuan fault zone, Ningxia Autonomous Region, China, and its

relation to the evolution of the north-eastern margin of the Tibet Plateau. *Tectonics*, *10*(6), 1091–1110.

Burgess, D. W. (1993). Automatic ship detection in satellite multispectral imagery. *Photogrammetric Engineering & Remote Sensing*, *59*(2), 229–237.

Carol, E., Braga, F., Donnici, S., Kruse, E., & Tosi, L. (2017). The hydrologic landscape of the Ajó coastal plain, Argentina: An assessment of human-induced changes. *Anthropocene*, *18*, 1–14.

Chen, H., Hu, J. M., Gong, W. B., Kang, R., & Li, L. B. (2015). Characteristics and transition mechanism of late Cenozoic structural. *Journal of Asian Earth Sciences*, *114*, 73–88.

Chen, X. L., Fan, T. L., Zhang, F., & Fan, Y. X. (2013). Formation of the Yellow River terraces around the Ordos Plateau and its relationship with uplift of Qinghai–Tibet Plateau. *Progress in Geography*, *32*(4), 595–605. (in Chinese with English abstract)

Deng, Q. D., Cheng, S. P., Ma, J., & Du, P. (2014). Seismic activities and earthquake potential in the Tibetan Plateau. *Chinese Journal of Geophysics*, *57*(5), 678–697.

Deng, Q. D., & You, H. C. (1985). Fault scarps research and earthquake risk estimation-example in eastern Helanshan fault scarps. *Northwestern Seismological Journal*, *7*(1), 29–38. (in Chinese with English abstract)

Feng, S. Y., Gao, R., Long, C. X., Fang, S. M., Zhao, C. B., Yan, K. P., ... He, H. Y. (2011). The compressive stress field of the Yinchuan garben: Deep seismic reflection profile. *Chinese Journal of Geophysics*, *54*(3), 692–697. (in Chinese with English abstract)

Fu, J. L., Zhang, W., Ma, Z. W., Wang, S. B., & Wu, Y. M. (2013). The terrace (T5 and T4) formation since the late Middle Pleistocene and its implication in the through cutting of the middle reach of Yellow River. *Earth Science Frontiers*, *20*(4), 166–181. (in Chinese with English abstract)

Gaudemer, Y., Tapponnier, P., Peltzer, G., Meyer, B., Guo, S., Chen, Z., ... Cifuentes, I. (1995). Partitioning of crustal slip between linked, active faults in the eastern Qilian Shan, and evidence for a major seismic gap, the 'Tianzhu gap', on the western Haiyuan Fault, Gansu (China). *Geophysical Journal International*, *120*(3), 599–645.

Geological Survey Institute of Ningxia Hui Autonomous Region (2018). *The regional geology of China·Ningxia* (pp. 307–320). Beijing: Geological Publishing House. (in Chinese)

Gong, W. B., Shi, W., Chen, H., Qiu, S. D., Yin, Y. G., & Zhao, W. (2016). Quaternary activity characteristics of the Liumugao fault in the northern section of Niushoushan-Luoshan fault. *Journal of Geomechanics*, *22*(4), 1004–1014. (in Chinese with English abstract)

Hooke, J. M. (1979). An analysis of the processes of river bank erosion. *Journal of Hydrology*, *42*, 39–62.

Hooke, J. M. (1980). Magnitude and distribution of rates of river bank erosion. *Earth Surface Processes*, *5*, 143–157.

Hu, Z. B., Li, M. H., Dong, Z. J., Guo, L. Y., Bridgland, D., Pan, B. T., ... Liu, X. F. (2019). Fluvial entrenchment and integration of the Sanmen Gorge, the Lower Yellow River. *Global and Planetary Change*, *178*, 129–138.

Hu, Z. B., Pan, B. T., Bridgland, D., Vandenberghe, J., Guo, L. Y., Fan, Y. L., & Westaway, R. (2017). The linking of the upper-middle and lower reaches of the Yellow River as a result of fluvial entrenchment. *Quaternary Science Reviews*, *166*(15), 324–338.

Huo, F. C., Pan, X. S., & You, G. L. (1989). *Introduction to Ningxia geology* (pp. 1–290). Beijing: Science Press. (in Chinese with English abstract)

Jackson, J., Norris, R., & Youngsun, J. (1996). The structural evolution of active fault and fold systems in central Otago, New Zealand: Evidence revealed by drainage patterns. *Journal of Structural Geology*, *18*, 217–234.

Jessica, Q., Shuhab, D. K., Mohamed, S. F., Abdel-Fattah, A., & Z. (2013). Remote sensing, planform, and facies analysis of the Plain of Tineh, Egypt for the remains of the defunct Pelusiac River. *Sedimentary Geology*, *297*, 16–30.

Jiang, Y. F., Yin, G. M., Yu, G., & Wang, C. (2013). Genetic-analysis of the Yellow River Big Bend in Shapotou Area, Ningxia Hui Autonomous Region. *China Earthquake Engineering Journal*, *35*(3), 631–640. (in Chinese with English abstract)

Knight, R. L., & Kadlec, R. H. (2000). Consuucted treatment wetland. *Water Global Technology*, *21*, 57–59.

Knighton, D. (1998). Fluvial forms and processes. In *A New Perspective* (Vol. 383). London: Arnold.

Kong, X. H., Bi, S. P., Liu, J., Song, X. S., Xu, C. F., & Ma, X. H. (2016). Geomorphological characteristics of paleo channel system in the last glacial maximum in the west of the South Yellow Sea shelf. *Marine Geology and Quaternary Geology*, *36*(6), 123–133. (in Chinese with English abstract)

Kou, Y. Q., & Du, D. L. (1995). Sedimentary features of shallow ancient river channels on the northern shelf of the South China Sea. *Acta Geologica Sinica (English Edition)*, *8*(1), 85–98.

Lacassin, R., Replumaz, A., Leloup, P., & Herv, E. (1998). Hairpin river loops and slip-sense inversion on Southeast Asian strike-slip faults. *Geology*, *26*(8), 703–706.

Laubel, A., Kronvang, B., Hald, A. B., & Jensen, C. (2003). Hydromorphological and biological factors influencing sediment and phosphorus loss via bank erosion in small lowland rural streams in Denmark. *Hydrological Processes*, *17*(17), 3443–3463.

Lawler, D. M. (1992). Process dominance in bank erosion systems. In P. Carling, & G. E. Petts (Eds.), *Lowland floodplain rivers: Geomorphological perspectives* (pp. 117–143). Chichester: Wiley.

Lawler, D. M. (1995). The impact of scale on the processes of channel-side sediment supply: A conceptual model. In Effects of Scale on the Interpretation and Management of Sediment and Water Quality. *Process symposium Boulder*, *226*, 175–184.

Lawler, D. M., Couperthwaite, J. S., Bull, L. J., & Harris, N. M. (1997). Bank erosion events and processes in the Upper Severn basin. *Hydrology and Earth System Sciences*, *1*(3), 523–534.

Liang, H., Zhang, W., Fu, J. L., Li, L. B., Chen, J., & Lu, K. (2013). The neotectonic in the Niushou Mountains, the northeast margin of the Tibetan Plateau, China and its impact on the evolution of the Yellow River. *Earth Science Frontiers*, *20*(4), 182–189. (in Chinese with English abstract)

Lin, A. M., Maruyama, T., & Miyata, T. (1998). Paleoseismic events and the 1596 Keicho-Fushimi large earthquake produced by a slip on the Gosukebashi fault at the eastern Rokko Mountains Japan. *The Island Arc*, *7*, 621–636.

Lin, A. M., Yang, Z. Y., Sun, Z. M., & Yang, T. S. (2001). How and when did the Yellow River develop its square bend? *Geology*, *9*(10), 951–954.

Liu, B. J., Feng, S. Y., Ji, J. F., Wang, S. J., Zhang, J. S., Yuan, H. K., & Yang, G. J. (2017). Lithospheric structure and faulting characteristics of the Helan Mountains and Yinchuan Basin Results of deep seismic reflection profiling. *Science China Earth Sciences*, *60*(3), 589–601.

Liu, B. W., Liu, X. F., Yuan, D. Y., Zheng, W. J., Guo, H., & Cao, J. J. (2003). Quaternary tectonic activities in northeastern Qinghai-Xizang Plateau as reflected by river terraces along the middle-upper reach of the Yellow River. *Seismology and Geology*, *25*(1), 133–145. (in Chinese with English abstract)

Liu, S. H., Feng, A. P., Liu, C. G., Zheng, Y. P., Li, P. Y., & Zhang, Z. W. (2018). Seismic stratigraphy and morphology of the Holocene progradational system beneath Bohai Bay, Bohai Sea: Lobate evolution of a multi-sourced subaqueous fluviodeltaic complex. *Marine Geology*, *409*, 31–47.

Liu, X. B., Hu, J. M., Shi, W., Chen, H., & Yan, J. Y. (2019). Palaeogene-Neogene sedimentary and tectonic evolution of the Yinchuan Basin, western North China Craton. *International Geology Review*. https://doi.org/10.1080/00206814.2019.1591309

Liu, X. B., Shi, W., Hu, J. M., Fu, J. L., Yan, J. Y., & Sun, L. L. (2019). Magnetostratigraphy and tectonic implications of Paleogene–Neogene sediments in the Yinchuan Basin, western North China Craton. *Journal of Asian Earth Sciences*, 173, 61–69.

Maruyama, T., & Lin, A. (2000). Tectonic history of the Rokko active fault zone (southwest Japan) inferred from the accumulative offset stream channels and basement rocks. *Tectonophysics*, 323, 197–216.

Molnar, P., & Tapponnier, P. (1975). Cenozoic tectonics of Asia, effects of a continental collision. *Science*, 189(4201), 419–426.

Pan, B. T., Hu, Z. B., Wang, J. P., Vandenberghe, J., Hu, X. F., Wen, Y. H., ... Cao, B. (2012). The approximate age of the planation surface and the incision of the Yellow River. *Palaeogeography, Palaeoclimatology, Palaeoecology*, 356-357, 54–61.

Pan, B. T., Liu, X. F., Gao, H. S., Wang, Y., & Li, J. J. (2007). The age of the river terraces in the upper reaches of the Weihe River and its genesis. *Progress in Natural Science*, 17(8), 1063–1068. (in Chinese with English abstract)

Pan, B. T., Wang, J. P., Gao, H. S., Guan, Q. Y., Wang, Y., Su, H., ... Li, J. J. (2005). Paleomagnetic dating of the topmost terrace in Kouma, Henan and its indication to the Yellow River's running through Sanmen Gorges. *Chinese Science Bulletin*, 50, 657–664.

Peltzer, G., Tapponnier, P., Zhang, Z., & Xu, Z. (1985). Neogene and Quaternary faulting in and along the Qinling Shan. *Nature*, 317, 500–505.

Poongodi, R., & Venkateswaran, S. (2018). Prioritization of the microwatersheds through morphometric analysis in the Vasishta Sub Basin of the Vellar River, Tamil Nadu using ASTER Digital Elevation Model (DEM) data. *Data in Brief*, 20, 1353–1359. https://doi.org/10.1016/j.dib.2018.08.197

Potter, P. E. (1978). Significance and origin of big rivers. *Journal of Geology*, 86, 13–33.

Schumm, S. A., Dumont, J. F., & Holbrook, J. M. (2000). *Active tectonics and alluvial rivers: Cambridge* (p. 376). UK: Cambridge University Press.

Shen, X. M., Tian, Y. T., Li, D. W., Qin, S. W., Vermeesch, P., & Schwanethal, J. (2016). Oligocene-Early Miocene river incision near the first bend of the Yangtze River: Insights from apatite (U-Th-Sm)/He thermochronology. *Tectonophysics*, 687, 223–231.

Shi, W., Dong, S. W., Liu, Y., Hu, J. M., Chen, X. H., & Chen, P. (2015). Cenozoic tectonic evolution of the South Ningxia region, northeastern Tibetan Plateau inferred from new structural investigations and fault kinematic analyses. *Tectonophysics*, 649, 139–164.

Su, Q., Ren, Z. K., Zhang, H. P., Zhang, P. Z., & Pichawut, M. (2019). The role of the Haiyuan Fault in accelerating incision rate of the Yellow River at the Mijia Shan Area, northeastern Tibetan Plateau, as revealed by in-situ [10]Be dating. *Journal of Asian Earth Sciences*, 179, 276–286.

Tapponnier, P. (1986). A tale of continents –The collision of great landmasses and the death of a sea are parts of the geological drama that created the Himalaya. *Natural History*, 95(11), 56–65.

Trimble, S. W. (1994). Erosional effects of cattle on streambanks in Tennesseep, USA. *Earth Surface Processes and Landforms*, 19, 451–464.

Wang, W. T., Zhang, P. Z., & Lei, Q. Y. (2013). Deformation characteristics of Niushoushan-Luoshan fault zone and its tectonic implications. *Seismology and Geology*, 35(2), 195–207. (in Chinese with English abstract)

Wu, G. F., Leeuw, J., Skidmore, A. K., Prins, H. H. T., & Liu, Y. L. (2007). Concurrent monitoring of vessels and water turbidity enhances the strength of evidence in remotely sensed dredging impact assessment. *Water Research*, 41(15), 3271–3280. https://doi.org/10.1016/j.watres.2007.05.018

Xing, C. Q., Yin, G. M., Ding, G. Y., Lu, Y. C., Shen, X. H., Tian, Q. J., ... Wei, K. B. (2002). Thickness of calcium carbonate coats on stones of the Heishanxia terraces of the Yellow River and dating of coarse clastic sedimentary geomorphic surfaces. *Chinese Science Bulletin*, 47(19), 1594–1600.

Yan, M. C., & Dong, G. R. (1997). Terraces development of Yellow River and geomorphic evolution in Shapotou area. *Journal of Desert Research*, 17(4), 369–376. (in Chinese with English abstract)

Yin, Z. Q., Qin, X. G., Liu, J. L., & Qiu, S. W. (2006). Formation background of the Zhalong wetland and its eco- environmental significance. *Progress in Geography*, 25(3), 32–38. (in Chinese with English abstract)

Zhang, J., Ma, Z. J., Lei, Y. L., & Ren, W. J. (2003). Structural characteristics in the Niushoushan area, central ningxia and its geological significance. *Geotectonics and Metallogenesis*, 27(2), 132–142. (in Chinese with English abstract)

Zhang, K., Liu, K. J., & Yang, J. C. (2004a). Asymmetrical valleys created by the geomorphic response of rivers to strike-slip fault. *Quaternary Research*, 62, 310–315.

Zhang, K., Liu, K. Y., Wu, J. M., Yang, J. C., & Cai, J. B. (2004b). Depositional features of the Zhongwei Basin, Ningxia, and its implication for Neotectonic movements. *Acta Sedimentologica Sinica*, 22(3), 465–473.

Zhang, P. Z., Molnar, P., Burchfiel, B. C., Royden, L. H., Wang, Y., Deng, Q., ... Jiao, D. (1988). Bounds on the Holocene sliprate of the Haiyuan fault, north-central China. *Quaternary Research*, 30, 151–164.

Zhang, Y. Q., Mercier, J. L., & Vergdly, P. (1998). Extension in the graben systems around the Ordos (China), and its contribution to the extrusion tectonics of south China with respect to Gobi-Mongolia. *Tectonophysics*, 285, 41–75.

Zhao, X. T., Jia, L. Y., & Hu, D. G. (2018). Discoveries of fluvial terraces and Neogene gravels in the Hetao area, inner Mongolia: Implications for the development of the Yellow River, antiquity of Chinese rivers, and coexistence theory of rivers and lakes. *Acta Geologica Sinica*, 92(4), 845–886.

Zhou, T. X., Wang, L., & Cao, M. Z. (1985). Morphotectonic patterns of Ningxia Hui-Autonomous region and its formation and evolution. *Acta Geographica Sinica*, 40(3), 215–224. (in Chinese with English abstract)

Zhou, T. X., Yao, M. W., & Wang, L. (1994). *Ningxia tectonic geomorphology*. Yinchuan: Ningxia People's Publishing House. (in Chinese with English abstract)